Atmos. Chem. Phys. Discuss., 14, 8695–8722, 2014
www.atmos-chem-phys-discuss.net/14/8695/2014/
doi:10.5194/acpd-14-8695-2014


Atmospheric Chemistry and Physics Discussions



# Application of positive matrix factor analysis in heterogeneous kinetics studies: an improvement to the mixed-phase relative rates technique

**Y. Liu, S.-M. Li, and J. Liggio**

Air Quality Processes Research Section, Environment Canada, Toronto, M3H 5T4, Canada

Received: 14 March 2014 – Accepted: 21 March 2014 – Published: 31 March 2014

Correspondence to: J. Liggio (john.liggio@ec.gc.ca)

Published by Copernicus Publications on behalf of the European Geosciences Union.







## Abstract

The mixed-phase relative rate approach for determining aerosol particle organic component heterogeneous reaction kinetics and OH uptake coefficients to particles is often performed utilizing mass spectral tracers as a proxy for particle phase reactant concentration. However, this approach may be influenced by signal contaminations from oxidation products during the experiment. In the current study, the mixed-phase relative rates technique has been improved by combining a Positive Matrix Factor (PMF) analysis with electron ionization Aerosol Mass Spectrometry, thereby removing the influence of $m/z$ fragments from reaction products on the reactant signals. To demonstrate the advantages of this approach, the heterogeneous reaction between OH radicals and citric acid (CA) was investigated using a photochemical flow tube coupled to a compact time-of-flight aerosol mass spectrometer (C-ToF-AMS). The measured heterogeneous rate constant ($k_2$) of citric acid toward OH was $(3.31 \pm 0.29) \times 10^{-12}$ cm$^3$ molecule$^{-1}$ s$^{-1}$ at 298 K and $(30 \pm 3)$ % RH and was $\sim 7.7$ times greater than previously reported results utilizing individual $m/z$ fragments. This phenomenon was further confirmed for particulate-phase organophosphates (TPhP, TDCPP, and TEHP), leading to $k_2$ values significantly larger than previously reported. The results suggest that heterogeneous kinetics can be significantly underestimated when a non-molecular ion peak is used as the tracer. Finally, the results suggest that the heterogeneous lifetime of organic aerosol in models can be overestimated due to underestimated OH uptake coefficients, and that it may be necessary to revisit the heterogeneous kinetic data of organic aerosol components which were derived in the context of the relative rates technique.

## 1 Introduction

Reaction kinetics data provide key parameters for both air quality and climate models. They are required to compute the trace gas and particle matter (PM) content of the atmosphere (Kolb et al., 2010) and to evaluate the atmospheric lifetime and fate for





ACPD
14, 8695–8722, 2014



individual species. Organic particle makes up 10–90 % of the global submicron particle mass in the lower troposphere (Zhang et al., 2011), and is comprised of various reactive organic species, which are subject to atmospheric heterogeneous oxidation. Previous studies have found that heterogeneous reactions with OH in particular, can lead to an increase in density, CCN activation (George and Abbatt, 2010) and optical extinction (Cappa et al., 2011) of organic particulate matter. Therefore, there is a growing interest in understanding not only the mechanism of PM transformation through heterogeneous reactions including oxidation, but also determining the rates at which organic aerosols are chemically transformed in the atmosphere.

To this end, Hearn and Smith (2006) developed a mixed-phase relative rate technique for measuring organic PM component heterogeneous reaction kinetic rate constants. In this method, the rate constant of the compound of interest is determined from the decrease of its particle phase relative concentration as a function of oxidant exposure. The oxidant levels are simultaneously estimated via the measured loss of a gas phase reference compound after applying the known second-order rate constant ($k_2$) toward the oxidant. In this approach the rates of chemical change are given by,

$$-\frac{\mathrm{d}c_\mathrm{A}}{\mathrm{d}t} = k_{2,\mathrm{A}} c_\mathrm{A} c_\mathrm{Ox} \quad (1)$$

$$-\frac{\mathrm{d}c_\mathrm{R}}{\mathrm{d}t} = k_{2,\mathrm{R}} c_\mathrm{R} c_\mathrm{Ox} \quad (2)$$

where $c_\mathrm{A}$, $c_\mathrm{R}$ and $c_\mathrm{Ox}$ are the particle phase concentration of the compound of interest (A), the gas phase concentration of the reference compound (R) and oxidant (molecules $\mathrm{cm}^{-3}$) respectively, while $k_{2,\mathrm{A}}$ and $k_{2,\mathrm{R}}$ are the second-order rate constant of A and R to the oxidant ($\mathrm{cm}^3\,\mathrm{molecule}^{-1}\,\mathrm{s}^{-1}$). A relative rate constant ($k_\mathrm{r}$) (i.e.: particle phase reaction rate of A, relative to the gas phase rate of R) can be derived by dividing Eq. (1) by Eq. (2). The derivation of $k_\mathrm{r}$ provides a means to obtain heterogeneous kinetic data without the need to know the absolute concentration of the oxidant. The differential and integral forms for the relative rates technique are shown as Eq. (3)





ACPD
14, 8695–8722, 2014



and Eq. (4),

$$\frac{dc_A}{c_A} = \frac{k_{2,A}}{k_{2,R}} \frac{dc_R}{c_R} = k_r \frac{dc_R}{c_R} \quad (3)$$

$$\log \frac{c_A}{c_{A,0}} = k_r \log \frac{c_R}{c_{R,0}} \quad (4)$$

from which the relative rate constant ($k_r$), is the slope of the line derived by plotting the logarithmic relative concentration of A against that of R (relative to initial conditions; $C_{A,0}$). The second-order heterogeneous rate constant of the compound of interest ($k_{2,A}$) towards the oxidant may then be calculated using the obtained $k_r$ and the known $k_{2,R}$ (i.e.: $k_{2,A} = k_r \times k_{2,R}$).

Using this method, a number of studies have quantified the uptake coefficients of $O_3$, OH, Cl, and $NO_3$ on various organic particles, and the corresponding second order rate constants for the degradation of organic compounds (George et al., 2007; Hearn and Smith, 2006; Kessler et al., 2012, 2010; Lambe et al., 2007; Liu et al., 2012; McNeill et al., 2007, 2008; Renbaum and Smith, 2011; Sareen et al., 2013; Smith et al., 2009).

Quantifying the particle phase loss of an organic compound in such studies often relies upon aerosol mass spectrometry techniques to monitor specific particle phase reactant ions of interest in semi-real time. Aerosol mass spectrometry instruments utilizing soft ionization techniques, such as chemical ionization (Aerosol CIMS) (Hearn and Smith, 2006; McNeill et al., 2007, 2008; Renbaum and Smith, 2011; Sareen et al., 2013) and vacuum ultraviolet photo-ionization (VUV-ATOFMS) (Liu et al., 2012), have been utilized to measure the concentration of the target organic compounds in particles. However, Aerosol Time-of-Flight or Quadrupole Mass Spectrometry (ToF-AMS or Q-AMS) employing electronic ionization (EI; 70 eV) as an ion source remains the prevalent instrument used in such organic particle experiments. In utilizing this approach, a specific fragment is often chosen as a tracer for the particle phase compound of interest. For example, $m/z$ 297 has been selected as a tracer for bis(2-ethylhexyl) sebacate (BES) (George et al., 2007), $m/z$ 71 for hexacosane (Lambe et al., 2007), $m/z$





ACPD
14, 8695–8722, 2014



113 for squalane (Smith et al., 2009), $m/z$ 104 and 144 for erythritol and levoglucosan (Kessler et al., 2010), and $m/z$ 152, 68 and 98 for 1,2,3,4-butanetetracarboxylic acid, citric acid and tartaric acid (Kessler et al., 2012) respectively.

However, the use of EI in conjunction with a particle vaporizer in the AMS results in heavy fragmentation for organic compounds due to the high energy associated with the EI source (70 eV) and the high temperature (~ 873 K) of the vaporizer (Allan et al., 2003; Jayne et al., 2000). Under such conditions, the tracer $m/z$ fragment is prone to interferences due to (1) the fragmentation of larger ions and/or molecules and (2) fragments from particle phase oxidation products. Both can contribute to the tracer $m/z$ signal, leading to an insensitive or nonlinear response of the tracer $m/z$ to the concentration of the target reactant during oxidation. The same may also be true for the $m/z$ for the molecular ion should one exist. Although it is often assumed that the chosen tracer ion does not contribute significantly to the mass spectra of any possible oxidation products or vice versa (Kessler et al., 2010), this is not always the case. In our previous work, we observed that the magnitude of the second order heterogeneous rate constant ($k_2$) increases as a function of increasing $m/z$ of the fragment chosen as a tracer of the parent molecule (Liu et al., 2014). This suggests an interference from the fragments selected, and points to the necessity to separate the signals of the compound of interest, from other compounds (products and/or fragment) for kinetic studies.

In the current study, we improve the mixed-phase relative rate technique used for studies of the heterogeneous oxidation of organic aerosol (OA) using positive matrix factorization (PMF) analysis of AMS derived kinetic data. Heterogeneous kinetics of citric acid (CA) toward OH oxidation was studied in a photo-chemical flow tube coupled to an Aerodyne C-ToF-AMS and an Ionicon Analytik High Resolution Proton Transfer Reaction Mass Spectrometer (PTR-ToF-MS). PMF analysis was used to successfully deconvolve the full mass spectra of the reactant from the potential oxidation products, hence allowing proper accounting of the time evolution of reactant concentrations during photochemical oxidation.





ACPD
14, 8695–8722, 2014



## 2 Experimental details

### 2.1 Flow tube experiments

A detailed schematic representation of the experimental system utilized in this study has been described elsewhere (Liu et al., 2014). Briefly, organic particles (citric acid) were generated via atomization (model 3706, TSI), dried through a diffusion drier and size-selected with a differential mobility analyzer (DMA) (model 3081, TSI). The dried, monodispersed CA particles were introduced into the flow tube reactor and exposed to differing OH concentrations. OH radicals were produced by the photolysis of $O_3$ at 254 nm in the presence of water vapor. $O_3$ was generated by passing zero air through an $O_3$ generator (OG-1, PCI Ozone Corp.). The $O_3$ concentration in the reactor was measured using an $O_3$ monitor (model 205, 2B Technologies) and ranged from 0–1000 ppbv. Relative humidity (RH) in the reactor was held constant (30±3) % by varying the ratio of wet to dry air used as an air source, and was measured at the exit of the flow tube reactor. The temperature was held constant at 298 K by circulating a temperature controlled fluid through the outer jacket of the reactor. The steady-state OH exposures were varied from 0 to $\sim 7.0 \times 10^{11}$ molecules $cm^{-3}$ s which was estimated on the basis of the decay of methanol from (as a reference compound) its reaction with OH. The decay of methanol from its reaction with OH was measured using the PTR-ToF-MS. The $k_2$ of methanol, $9.4 \times 10^{-13}$ $cm^3$ $molecule^{-1}$ $s^{-1}$, was used for the OH exposure calculation (Atkinson and Arey, 2003).

OH radical reactions were performed in a custom-made reactor consisting of two electro-polished stainless steel cylinders with inner diameter of 7.3 cm. The first stage contained static mixing elements (StaMixCo) to ensure that particles and gas phase species were well mixed prior to entering the reaction region (second stage). Fluid dynamics simulations of the flow tube confirmed that particles and gas phase species were well mixed in the reactor, with a uniform initial velocity profile. The size and composition of the particles exiting the reactor were measured by a scanning mobility particle sizer (SMPS, TSI) and an Aerodyne C-ToF-AMS (Drewnick et al., 2005).





ACPD
14, 8695–8722, 2014



Control experiments demonstrated that $O_3$ or 254 nm light exposure did not lead to the decomposition of CA. Analytic grade CA (EM, Germany) was used as received. 18.2 MΩ water was used as solvent.

### 2.2 PMF analysis and kinetics calculation

PMF is a multivariate factor analysis tool that decomposes a matrix of speciated sample data into two matrices, namely, factor contributions and factor profiles (Paatero and Tapper, 1994), such that

$$x_{ij} = \sum_{p} g_{ip} f_{pj} + e_{ij} \quad (5)$$

Where $i$ and $j$ refer to row and column indices in the matrix, respectively, $p$ is the number of factors in the solution, $x_{ij}$ is an element of the $m \times n$ matrix **X** of measured data elements to be fit, and $e_{ij}$ is the residual. Results are constrained so that no sample can have a negative source contribution. The PMF solution minimizes the object function $Q$ (Eq. 6), based upon the uncertainties ($u$) (Norris and Vedantham, 2008).

$$Q = \sum_{i=1}^{n} \sum_{j=1}^{m} \left( \frac{e_{ij}}{u_{ij}} \right)^2 \quad (6)$$

Its ability to separate the signals of a multi-component matrix has been well established. PMF analysis has been widely used for source apportionment of ambient particles in field measurements (Liggio et al., 2010; Schwartz et al., 2010; Song et al., 2006; Ulbrich et al., 2009; Viana et al., 2008; Yuan et al., 2006). Three secondary organic aerosols (SOA1, SOA2, SOA3) have also been identified for OH initiated oxidation of laboratory SOA (George and Abbatt, 2010). Therefore, the use of PMF for separating the reactants from the products in laboratory studies aimed at using the relative rates method for heterogeneous kinetic studies would seem to be a reasonable approach.





ACPD
14, 8695–8722, 2014



The AMS data for CA oxidation from all experiments combined were used as input into the PMF Evaluation Toolkit (PET) v2.05 (Paatero, 1997; Paatero and Tapper, 1994) to separate the signals of CA and the corresponding oxidation products. In the AMS data, the $m$ rows of **X** are ensemble average mass spectra (MS) of typically tens of thousands of particles measured over each averaging period (typically 2 min) and the $n$ columns of **X** are the time series (TS) of each $m/z$ sampled.

PMF analyses were done in the robust mode. The default convergence criteria were not modified. The Q values as a function of FPEAK from −1 to +1 were examined (Reff et al., 2007). For the variables with signal-to-noise ratio (SNR) less than 0.2 ("bad" variables) and downweight variables with SNR between 0.2 and 2 ("weak" variables), their error estimates were increased by a factor of 10 and 3, respectively, as recommended by Paatero and Hopke (2003). In this study, the SNR of all $m/z$ fragments are larger than 0.2. The error values for $m/z$ 44, 18, 17 and 16 were multiplied by sqrt(4).

The extracted factor profiles (mass spectra for CA and the oxidation products) were compared with the NIST mass spectrum of pure CA and that measured with the C-ToF-AMS directly via atomization. The temporal concentration profiles (factor contributions) of CA were further confirmed via comparison to the known experimental conditions used for kinetics calculations (i.e.: zero OH exposure should result in a CA factor contribution of 100 %). For comparison with the PMF results, the kinetic rate constants ($k_r$) were also calculated using specific individual tracers of CA at $m/z$ 87, 129 and 147, separately. The $k_r$ of CA toward methanol was calculated according to Eq. (4). The $k_2$ of CA was further calculated with the known $k_2$ of methanol and $k_r$.

The reactive uptake coefficient of OH ($\gamma_{OH}$) with CA was calculated using the following formulation (Kessler et al., 2012, 2010; Liu et al., 2012; Worsnop et al., 2002):

$$\gamma_{OH} = \frac{2D_p \rho_{CA} N_A}{3v_{OH} M_{CA} k_2} \quad (7)$$





ACPD
14, 8695–8722, 2014



Where $D_p$ is the surface-weight average particle diameter of unreacted particles (cm), $\rho_{CA}$ is the density of CA ($g\,cm^{-3}$), $N_A$ is Avogadro's number, $v_{OH}$ is the average speed of OH radicals in the gas phase ($cm\,s^{-1}$), $M_{CA}$ is the molecular weight of CA ($g\,mol^{-1}$).

## 3 Results

### 3.1 PMF analysis of AMS data

To ensure that oxidation of CA in particles does not result in a PTR-ToF-MS response for methanol in the gas phase (thus compromising the OH radical reference measurement), the oxidation of pure CA was performed in the absence of methanol, with no gas phase methanol signal detected by the PTR-ToF-MS. The mass concentration of the OA measured with the AMS during oxidation is shown in Fig. 1a, which was constant. The results of Fig. 1a demonstrate that the aerosol source is adequately stable for kinetic studies to be performed.

A two factor solution from the PMF analysis accounts for ~ 85 % of the variance of the data. When the number of factors is greater than 2, none of the obtained factors resembles that of pure CA, whose contribution should be approximately 100 % when OH is absent in the reactor. Figure 1b and c represents the temporal variations of the typical 2-factor PMF solution of AMS data when CA is exposed to varying OH concentrations. The error bars indicate the rotational uncertainty in the PMF analysis. Three independent experiments were performed to test the response of CA signal to OH exposure (determined by $O_3$ concentration). In the first and the third experiments, OH exposure was stepped downwards (high to low OH) by changing the power of $O_3$-generator with the same flow rate and RH, while the inverse sequence was performed in the second experiment.

As demonstrated in Fig. 1b and c, in the absence of OH radical (labeled "0"), factor 1 (Fig. 1b) accounts for (94.7 ± 0.9) % of the OA mass, while factor 2 (Fig. 1c) contributes (6.2 ± 0.7) % of OA. This is consistent with the experimental conditions of zero OH





ACPD
14, 8695–8722, 2014



radical (i.e.: no oxidation), and suggests that factor 1 should be assigned to the citric acid reactant. Impurities in the CA or the water used to atomize CA likely contributed to factor 2. When OH exposure was decreased in a step-wise manner in the first and the third experiment (Fig. 1b), the extracted factor representative of CA (factor 1) increased synchronously, and is accompanied with a decrease in factor 2. Therefore, factor 2 is interpreted as the OH oxidation products of CA. This is consistent with the second experiment, where the inverse trend was observed with a step-wise OH exposure increase. Based upon this evidence, we conclude that changes in the time series of factors 1 and 2 extracted by PMF are consistent with the expected response to OH exposures, namely, that higher OH exposure resulted in a decrease in CA (factor 1) and an increase in the oxidation products (factor 2).

The factor profiles (i.e.: mass spectra) extracted by PMF analysis are shown in Fig. 2. The main fragments of CA including $m/z$ values 129 ($C_5H_5O_4^+$) and 87 ($C_3H_3O_3^+$) are present in factor 1 (Fig. 2a). These fragments are in good agreement with the NIST mass spectra of pure CA and the mass spectrum of pure CA particles measured with the C-ToF-AMS (Fig. 3). Figure 4 further compared the normalized mass spectra of factor 1 and pure CA directly measured with the C-ToF-AMS. The relative intensities for all ions of pure CA are linearly correlated with that of factor 1 with a slope of 0.985 and $R$ of 0.9999. This further confirmed that factor 1 should be assigned to unreacted CA. Figure 2c shows the difference mass spectra (factor 2 – factor 1). Consumption of $m/z$ values 147 ($C_5H_7O_5^+$), 129, 87, 85 ($C_4H_5O_2^+$), 68 ($C_4H_4O^+$) and 60 ($C_2H_4O_2^+$) can be observed, which is consistent with the assignment that factor 2 belongs to oxidation products of CA. However, small changes in the relative intensities of these peaks suggest that the structure of the oxidation products of CA are likely similar to that of CA. For example, as shown in Fig. 2a and b, the intensity of $m/z$ 129 and 87 in factor 2 are $0.0125 \pm 0.0046$ and $0.218 \pm 0.0013$ compared to $0.0141 \pm 0.0046$ and $0.235 \pm 0.0013$ in factor 1.

The changes of the relative concentrations of gas phase methanol and particle phase CA are shown in Fig. 5. The signal of CA extracted by PMF analysis also responded





ACPD
14, 8695–8722, 2014



to OH exposure as expected, when methanol was present in the gas phase, which is similar to that of Fig. 1. The relative intensities of the typical tracers of CA at $m/z$ 87, 129 and 147 are shown in Fig. 5c. However, the relative loss of these tracers as a function of OH exposure in Fig. 5c is much smaller than that of the CA factor derived from the PMF analysis (Fig. 5b). In addition, the consumption of the smaller tracer ($m/z$ 87) is substantially lower than that of the larger ones ($m/z$ values 129 and 147). For example, the maximum consumption of CA extracted with PMF analysis is approximately 80 %, in comparison to ∼ 30 %, ∼ 10 % and 5 % for $m/z$ values 147, 129 and 87, respectively. These results support the small differences in the mass spectra between the unreacted CA and its oxidation products as shown in Fig. 2. Furthermore, it suggests that the measured loss of these fragments, which were supposedly only derived from CA, had in fact contributions from the fragmentation of the products of CA oxidation. This ultimately would lead to an underestimation of the second order heterogeneous rate constant (or OH uptake coefficients) if these fragments were chosen as the proxies for the particle phase concentration of CA.

### 3.2 Reaction kinetics

The saturation vapor pressure of CA at 298 K is $1.6 \times 10^{-7}$ Pa (Huisman et al., 2013), thus 99.9 % of CA should be present in the particle phase under the current experimental conditions according to a partition model (Kroll and Seinfeld, 2008; Pankow, 1994). Although new particle formation was observed with a CPC in the experiments (at the exit of the reactor), it has no influence on the measured mass concentration of OA due to the small particle size of the new particles. This is well supported by the constant mass concentration of OA measured with the AMS during oxidation experiments (Fig. 1a). In addition, as pointed out in our previous work (Liu et al., 2014), evaporation of CA from particles could potentially contribute to the decreases in particle phase CA concentration observed as a function of OH exposure. If CA evaporation was at play, the derived reaction rates will be overestimated using either the present approach or the simpler methods of using single fragments. The evaporation of CA





ACPD
14, 8695–8722, 2014



from the particle phase under these experimental conditions from control experiments is less than 0.05 % based upon an evaporation model.(Rajagopal and Rao, 2004). This implies that the observed changes in CA concentration in the particle phase were due to the particle phase reaction.

The relative rates (relative to initial conditions) for CA and methanol in these experiments are shown in Fig. 6. The logarithmic $c/c_0$ of CA both measured with the tracers and extracted with PMF analysis linearly correlated to that of methanol with $R^2 > 0.95$. The derived relative rate constant based upon PMF analysis is $3.01 \pm 0.27$, while it is $0.72 \pm 0.05$ and $0.22 \pm 0.01$ for $m/z$ values 147 and 129, respectively. Applying the $k_2$ value of methanol towards OH of $9.4 \times 10^{-13}$ cm$^3$ molecule$^{-1}$ s$^{-1}$ at 298 K (Atkinson and Arey, 2003), the $k_2$ of CA is calculated as $(2.83 \pm 0.25) \times 10^{-12}$ using the PMF approach, or $(6.77 \pm 0.47) \times 10^{-13}$ using the single tracer at $m/z$ 147 and $(2.02 \pm 0.01) \times 10^{-13}$ cm$^3$ molecule$^{-1}$ s$^{-1}$ using the single tracer at $m/z$ 129, respectively. The reaction between methanol and OH radicals occurs in the gas phase, while for the CA oxidation it occurs in particle phase. Thus it is necessary to correct for OH diffusion from the bulk gas phase to the particle phase. Applying a diffusion correction utilizing a previously developed empirical formula (Fuchs and Sutugin, 1970; Widmann and Davis, 1997; Worsnop et al., 2002), the diffusion-corrected $k_2$ is $(3.31 \pm 0.29) \times 10^{-12}$ using the PMF approach, and $(7.92 \pm 0.55) \times 10^{-13}$ and $(2.36 \pm 0.01) \times 10^{-13}$ cm$^3$ molecule$^{-1}$ s$^{-1}$ using single tracers at $m/z$ 147 and 129, respectively. The diffusion-corrected $\gamma_{OH}$ is calculated as $2.74 \pm 0.24$ using the PMF approach, and $0.66 \pm 0.46$ and $0.20 \pm 0.01$ using single tracers at $m/z$ 147 and 129, respectively.

## 4 Discussion

Kessler et al. (2012) have reported the $k_2$ of CA toward OH to be $(4.3 \pm 0.8) \times 10^{-13}$ cm$^3$ molecule s$^{-1}$ at 308 K and 30 % RH with an Aerodyne AMS. In their work,





ACPD
14, 8695–8722, 2014



the diameter of particles and RH were equivalent to the current work, while their experimental temperature was 10 K higher. In addition, a fragment of $m/z$ 68 was used as the tracer of CA in their work. However, no significant consumption of $m/z$ 68 was observed in this study, which might be related to the difference in reaction temperature, and therefore $m/z$ 129 and 147 are used as tracers. The measured $k_2$ of CA utilizing $m/z$ 129 and 147 in this study is of the same order of magnitude as that reported in Kessler et al. (2012). However, as shown in Fig. 3c, the consumption of $m/z$ 87 is much lower than that of $m/z$ 129. The apparent $k_2$ of CA based on $m/z$ 87 is $(9.9 \pm 0.8) \times 10^{-14}$ cm$^3$ molecule$^{-1}$ s$^{-1}$, and the diffusion-corrected $k_2$ is $(1.16 \pm 0.09) \times 10^{-13}$ cm$^3$ molecule$^{-1}$ s$^{-1}$. This suggests that the derived rate constant greatly depends upon the size of the tracer fragment, with larger fragments resulting in larger values of $k_2$. This is consistent with our previous work for oxidation of triphenyl phosphate (TPhP) (Liu et al., 2014). The $k_2$ of CA based on PMF analysis is approximately an order of magnitude larger than the Kessler's result measured with the tracer at $m/z$ 68, and 4.2 times greater than that calculated based upon $m/z$ 147 in this study.

Citric acid is a hydroxyl substituted poly carboxyl acid. Scheme 1 summarizes its possible fragmentation pathways. The typical mass peaks including $m/z$ 147, 129, 87, 85 and 68 would result from this scheme and were indeed observed. Since the fragments at $m/z$ 129, 87, 85 and 68 are likely second or third (or even high) generation fragments, their signal intensities may be highly influenced by products and/or larger fragments. In some instances, oxidation products can exhibit similar fragmentation pathways as the reactants. This is likely the case for the smaller fragments of CA. For example, scheme 2 illustrates the possible fragmentation pathways of 2,3-dihydroxypropane-1,2,3-tricarboxylic acid, which is one of the products from the OH oxidation of citric acid (Atkinson, 1986). As observed in Scheme 2, there are several pathways leading to the fragment at $m/z$ 87, implying that the decrease in the signal of $m/z$ 87 due to CA oxidation is likely to be compensated by fragments from the oxidation products. In addition, it is also possible to form fragments with the same $m/z$ as





ACPD
14, 8695–8722, 2014



the parent citric acid if the dehydration reaction (the 6th path in Scheme 2) takes place initially.

The current relative rate method based upon PMF analysis was used to re-analyze the heterogeneous oxidation kinetics of three organophosphate flame retardants found in ambient particles and reported previously (Liu et al., 2014). The $k_2$ values for TPhP, tris-1,3-dichloro-2-propyl phosphate (TDCPP) and tris-2-ethylhexyl phosphate (TEHP) utilizing the tracer and PMF approaches are summarized in Table 1. For TPhP, its molecular ion peak ($M^+$; 326) was chosen as a tracer; while the largest detectable fragments, i.e. $m/z$ 381and 323, were chosen for TDCPP ($M^+$; 431) and TEHP ($M^+$; 435), respectively. The typical evolution of the PMF factors of TPhP, TDCPP, and TEHP are shown in Figs. S1–S3. For TPhP, the measured $k_2$ values derived by both methods are comparable within the experimental uncertainties, while $k_2$ of TDCPP and TEHP based upon PMF analysis is 1.5 and 1.6 times larger than that using the chosen tracers. The good agreement between methods for TPhP is likely due to the fact that the molecular ion peak ($M^+$) is measurable for TPhP with the AMS, while it is not observable for TDCPP, TEHP and CA. Therefore, the influence of secondary fragmentation from larger fragments has little influence on the signal of $M^+$ for TPhP. These results also demonstrate that a substantial underestimation of rate constants could result when a non-molecular ion tracer is used to monitor the particle phase concentration of organic matter with AMS for heterogeneous kinetic studies.

## 5 Implications and conclusions

An improvement in the mixed-phase relative rates technique is achieved based upon PMF analysis of AMS derived spectra. The measured $k_2$ for citric acid toward OH is $(3.31 \pm 0.29) \times 10^{-12}\,cm^3\,molecule^{-1}\,s^{-1}$ at 298 K and 30 % RH. This value is at least 4.2 times greater than that calculated on the basis of atypical tracer $m/z$ 147 or 7.7 times greater than the Kessler's value (Kessler et al., 2012). These results suggest that the heterogeneous kinetics of OA is substantially underestimated when a non-





ACPD
14, 8695–8722, 2014



molecular ion peak is used as the tracer to measure the particle phase concentration of OA. In model simulations, the reactive uptake coefficient of OH or other radicals, which are calculated based upon $k_2$, is an important parameter in evaluating the fate of OA during transport. The current results suggest that the lifetime of OA estimated in models due to heterogeneous oxidation might be overestimated when using kinetics data derived by using individual non-molecular $m/z$ tracers of OA, and that it may be necessary to revisit the kinetic data of other organic aerosol components (and OH uptake coefficients) which have been derived using the relative rates technique (George et al., 2007; Lambe et al., 2007).

**Supplementary material related to this article is available online at http://www.atmos-chem-phys-discuss.net/14/8695/2014/acpd-14-8695-2014-supplement.pdf.**

*Acknowledgements.* This research was funded by the Chemicals Management Plan (CMP) and the Clean Air Regulatory Agenda (CARA).

## References

Allan, J. D., Jimenez, J. L., Williams, P. I., Alfarra, M. R., Bower, K. N., Jayne, J. T., Coe, H., and Worsnop, D. R.: Quantitative sampling using an Aerodyne aerosol mass spectrometer 1. Techniques of data interpretation and error analysis, J. Geophys. Res., 108, 4090, doi:10.1029/2002JD002358, 2003.

Atkinson, R.: Kinetics and mechanisms of the gas-phase reactions of the hydroxyl radical with organic compounds under atmospheric conditions, Chem. Rev., 85, 69–201, 1986.

Atkinson, R. and Arey, J.: Atmospheric degradation of volatile organic compounds, Chem. Rev., 103, 4605–4638, 2003.

Cappa, C. D., Che, D. L., Kessler, S. H., Kroll, J. H., and Wilson, K. R.: Variations in organic aerosol optical and hygroscopic properties upon heterogeneous OH oxidation, J. Geophys. Res., 116, D15204, doi:10.1029/2011JD015918, 2011.





ACPD
14, 8695–8722, 2014



Drewnick, F., Hings, S. S., DeCarlo, P., Jayne, J. T., Gonin, M., Fuhrer, K., Weimer, S., Jimenez, J. L., Demerjian, K. L., Borrmann, S., and Worsnop, D. R.: A new Time-of-Flight Aerosol Mass Spectrometer (TOF-AMS) – instrument description and first field deployment, Aerosol Sci. Tech., 39, 637–658, 2005.

Fuchs, N. A. and Sutugin, A. G.: Highly Dispersed Aerosols, Butterworth-Heinemann, Newton, MA, 1970.

George, I. J. and Abbatt, J. P. D.: Chemical evolution of secondary organic aerosol from OH-initiated heterogeneous oxidation, Atmos. Chem. Phys., 10, 5551–5563, doi:10.5194/acp-10-5551-2010, 2010.

George, I. J., Vlasenko, A., Slowik, J. G., Broekhuizen, K., and Abbatt, J. P. D.: Heterogeneous oxidation of saturated organic aerosols by hydroxyl radicals: uptake kinetics, condensed-phase products, and particle size change, Atmos. Chem. Phys., 7, 4187–4201, doi:10.5194/acp-7-4187-2007, 2007.

Hearn, J. D. and Smith, G. D.: A mixed-phase relative rates technique for measuring aerosol reaction kinetics, Geophys. Res. Lett., 33, L17805, doi:10.1029/2006GL02693, 2006.

Huisman, A. J., Krieger, U. K., Zuend, A., Marcolli, C., and Peter, T.: Vapor pressures of substituted polycarboxylic acids are much lower than previously reported, Atmos. Chem. Phys., 13, 6647–6662, doi:10.5194/acp-13-6647-2013, 2013.

Jayne, J. T., Leard, D. C., Zhang, X., Davidovits, P., Smith, K. A., Kolb, C. E., and Worsnop, D. R.: Development of an aerosol mass spectrometer for size and composition analysis of submicron particles, Aerosol Sci. Tech., 33, 49–70, 2000.

Kessler, S. H., Smith, J. D., Che, D. L., Worsnop, D. R., Wilson, K. R., and Kroll, J. H.: Chemical sinks of organic aerosol: kinetics and products of the heterogeneous oxidation of erythritol and levoglucosan, Environ. Sci. Technol., 44, 7005–7010, 2010.

Kessler, S. H., Nah, T., Daumit, K. E., Smith, J. D., Leone, S. R., Kolb, C. E., Worsnop, D. R., Wilson, K. R., and Kroll, J. H.: OH-initiated heterogeneous aging of highly oxidized organic aerosol, J. Phys. Chem. A, 116, 6358–6365, 2012.

Kolb, C. E., Cox, R. A., Abbatt, J. P. D., Ammann, M., Davis, E. J., Donaldson, D. J., Garrett, B. C., George, C., Griffiths, P. T., Hanson, D. R., Kulmala, M., McFiggans, G., Pöschl, U., Riipinen, I., Rossi, M. J., Rudich, Y., Wagner, P. E., Winkler, P. M., Worsnop, D. R., and O' Dowd, C. D.: An overview of current issues in the uptake of atmospheric trace gases by aerosols and clouds, Atmos. Chem. Phys., 10, 10561–10605, doi:10.5194/acp-10-10561-2010, 2010.





ACPD
14, 8695–8722, 2014



Kroll, J. H. and Seinfeld, J. H.: Chemistry of secondary organic aerosol: formation and evolution of low-volatility organics in the atmosphere, Atmos. Environ., 42, 3593–3624, 2008.
Lambe, A. T., Zhang, J. Y., Sage, A. M., and Donahue, N. M.: Controlled OH radical production via ozone-alkene reactions for use in aerosol aging studies, Environ. Sci. Technol., 41, 2357–2363, 2007.
Liggio, J., Li, S. M., Vlasenko, A., Sjostedt, S., Chang, R., Shantz, N., Abbatt, J., Slowik, J. G., Bottenheim, J. W., Brickell, P. C., Stroud, C., and Leaitch, W. R.: Primary and secondary organic aerosols in urban air masses intercepted at a rural site, J. Geophys. Res., 115, D21305, doi:10.1029/2010JD014426, 2010.
Liu, C., Zhang, P., Wang, Y., Yang, B., and Shu, J.: Heterogeneous reactions of particulate methoxyphenols with $NO_3$ radicals: kinetics, products, and mechanisms, Environ. Sci. Technol., 46, 13262–13269, 2012.
Liu, Y., Liggio, J., Harner, T., Jantunen, L., Shoeib, M., and Li, S.-M.: Heterogeneous OH initiated oxidation: a possible explanation for the persistence of organophosphate flame retardants in air, Environ. Sci. Technol., 48, 1041–1048, 2014.
McNeill, V. F., Wolfe, G. M., and Thornton, J. A.: The oxidation of oleate in submicron aqueous salt aerosols: evidence of a surface process, J. Phys. Chem. A, 111, 1073–1083, 2007.
McNeill, V. F., Yatavelli, R. L. N., Thornton, J. A., Stipe, C. B., and Landgrebe, O.: Heterogeneous OH oxidation of palmitic acid in single component and internally mixed aerosol particles: vaporization and the role of particle phase, Atmos. Chem. Phys., 8, 5465–5476, doi:10.5194/acp-8-5465-2008, 2008.
Norris, G. and Vedantham, R.: EPA positive matrix factorization (PMF) 3.0 fundamentals & user guide, US Environmental Protection Agency, available at: http://www.epa.gov/heasd/research/pmf.html (last access: 9 August 2013), 2008.
Paatero, P.: Least squares formulation of robust non-negative factor analysis, Chemometr. Intell. Lab., 37, 23–35, 1997.
Paatero, P. and Hopke, P. K.: Discarding or downweighting highnoise variables in factor analytic models, Anal. Chim. Acta, 490, 277–289, 2003.
Paatero, P. and Tapper, U.: Positive matrix factorization: a nonnegative factor model with optimal utilization of error estimates of data values, Environmetrics, 5, 111–126, 1994.
Pankow, J. F.: An absorption-model of gas-particle partitioning of organic compounds in the atmosphere, Atmos. Environ., 28, 185–188, 1994.





ACPD
14, 8695–8722, 2014



Rajagopal, R. and Rao, Y. K.: Modeling of silicon vapor phase epitaxy using Stefan–Maxwell formalism, Mater. Trans., 45, 2395–2402, 2004.
Reff, A., Eberly, S. I., and Bhave, P. V.: Receptor modeling of ambient particulate matter data using positive matrix factorization, review of existing methods, J. Air Waste Manage., 57, 146–154, 2007.
Renbaum, L. H. and Smith, G. D.: Artifacts in measuring aerosol uptake kinetics: the roles of time, concentration and adsorption, Atmos. Chem. Phys., 11, 6881–6893, doi:10.5194/acp-11-6881-2011, 2011.
Sareen, N., Moussa, S. G., and McNeill, V. F.: Photochemical aging of light-absorbing secondary organic aerosol material, J. Phys. Chem. A, 117, 2987–2996, 2013.
Schwartz, R. E., Russell, L. M., Sjostedt, S. J., Vlasenko, A., Slowik, J. G., Abbatt, J. P. D., Macdonald, A. M., Li, S. M., Liggio, J., Toom-Sauntry, D., and Leaitch, W. R.: Biogenic oxidized organic functional groups in aerosol particles from a mountain forest site and their similarities to laboratory chamber products, Atmos. Chem. Phys., 10, 5075–5088, doi:10.5194/acp-10-5075-2010, 2010.
Smith, J. D., Kroll, J. H., Cappa, C. D., Che, D. L., Liu, C. L., Ahmed, M., Leone, S. R., Worsnop, D. R., and Wilson, K. R.: The heterogeneous reaction of hydroxyl radicals with sub-micron squalane particles: a model system for understanding the oxidative aging of ambient aerosols, Atmos. Chem. Phys., 9, 3209–3222, doi:10.5194/acp-9-3209-2009, 2009.
Song, Y., Zhang, Y., Xie, S., Zeng, L., Zheng, M., Salmon, L. G., Shao, M., and Slanina, S.: Source apportionment of $PM_{2.5}$ in Beijing by positive matrix factorization, Atmos. Environ., 40, 1526–1537, 2006.
Ulbrich, I. M., Canagaratna, M. R., Zhang, Q., Worsnop, D. R., and Jimenez, J. L.: Interpretation of organic components from Positive Matrix Factorization of aerosol mass spectrometric data, Atmos. Chem. Phys., 9, 2891–2918, doi:10.5194/acp-9-2891-2009, 2009.
Viana, M., Kuhlbusch, T. A. J., Querol, X., Alastuey, A., Harrison, R. M., Hopke, P. K., Winiwarter, W., Vallius, A., Szidat, S., Prevot, A. S. H., Hueglin, C., Bloemen, H., Wahlin, P., Vecchi, R., Miranda, A. I., Kasper-Giebl, A., Maenhaut, W., and Hitzenberger, R.: Source apportionment of particulate matter in Europe: a review of methods and results, J. Aerosol Sci., 39, 827–849, 2008.
Widmann, J. F. and Davis, E. J.: Mathematical models of the uptake of $ClONO_2$ and other gases by atmospheric aerosols, J. Aerosol Sci., 28, 87–106, 1997.





ACPD
14, 8695–8722, 2014



Worsnop, D. R., Morris, J. W., Shi, Q., Davidovits, P., and Kolb, C. E.: A chemical kinetic model for reactive transformations of aerosol particles, Geophys. Res. Lett., 29, 1996, doi:10.1029/2002GL015542, 2002.

Yuan, Z. B., Yu, J. Z., Lau, A. K. H., Louie, P. K. K., and Fung, J. C. H.: Application of positive matrix factorization in estimating aerosol secondary organic carbon in Hong Kong and its relationship with secondary sulfate, Atmos. Chem. Phys., 6, 25–34, doi:10.5194/acp-6-25-2006, 2006.

Zhang, Q., Jimenez, J., Canagaratna, M., Ulbrich, I., Ng, N., Worsnop, D., and Sun, Y.: Understanding atmospheric organic aerosols via factor analysis of aerosol mass spectrometry: a review, Anal. Bioanal. Chem., 401, 3045–3067, 2011.





ACPD
14, 8695–8722, 2014



**Table 1.** Comparison of the measured $k_2$ values utilizing PMF and select $m/z$ tracers, for organophosphate compounds and CA.

| OA | Mean $k_{r\_PMF}$ | $k_2$ ($10^{12}$) cm$^3$ molecule$^{-1}$ s$^{-1}$ | | | $k_{2\_PMF}/k_{2\_Tracer}$ | $M_{Tracer}/M^+$ |
|---|---|---|---|---|---|---|
| | | $k_{2,obs\_PMF}$ | $k_{2,t\_PMF}$ | $k_{2,t\_Tracer}$ | | |
| TPhP | $1.58 \pm 0.33$ | $1.48 \pm 0.31$ | $1.95 \pm 0.43$ | $2.10 \pm 0.19^*$ | 0.9 | 326/326 |
| TDCPP | $1.20 \pm 0.31$ | $1.13 \pm 0.29$ | $1.35 \pm 0.35$ | $0.92 \pm 0.09^*$ | 1.5 | 381/431 |
| TEHP | $3.52 \pm 0.65$ | $3.31 \pm 0.61$ | $4.25 \pm 0.78$ | $2.70 \pm 0.63^*$ | 1.6 | 323/435 |
| CA | $3.01 \pm 0.27$ | $2.83 \pm 0.25$ | $3.31 \pm 0.29$ | $0.79 \pm 0.06$ | 4.2 | 147/192 |

* Liu et al. (2014).





ACPD
14, 8695–8722, 2014



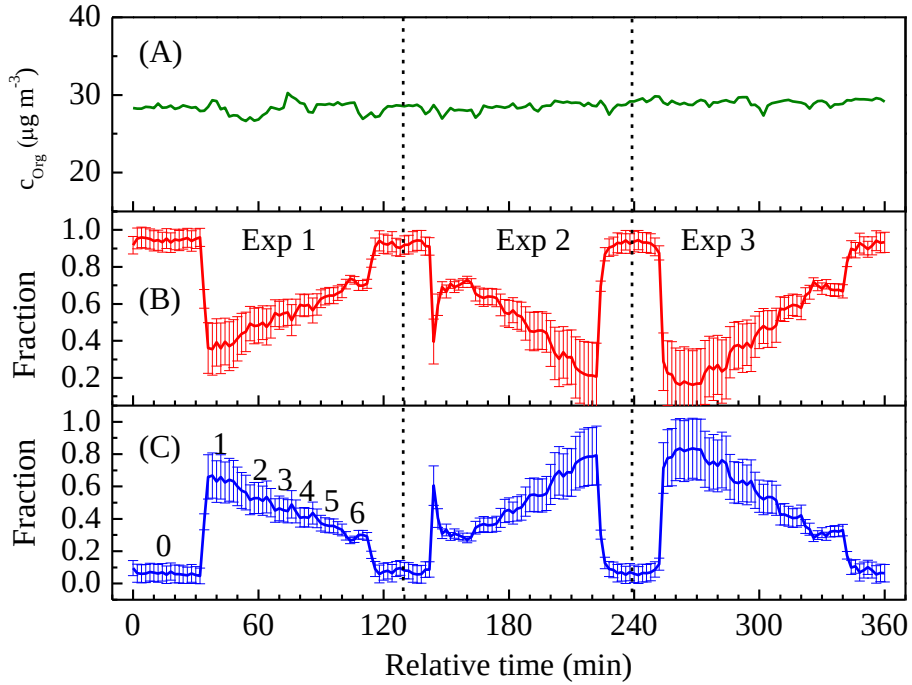


**Fig. 1.** Changes in **(A)** total organic mass concentration, **(B)** the fraction of unreacted citric acid derived by PMF and **(C)** products of citric acid oxidized by OH derived by PMF, as a function of relative experimental time. The values 1–6 represent a step-wise $O_3$ concentration decrease, corresponding to decreased OH exposure; 0 represents an $O_3$ concentration of zero. Experimental conditions are $D_m$: 200 nm, RH: 30 ± 3 %, $T$: 298 K.





ACPD
14, 8695–8722, 2014



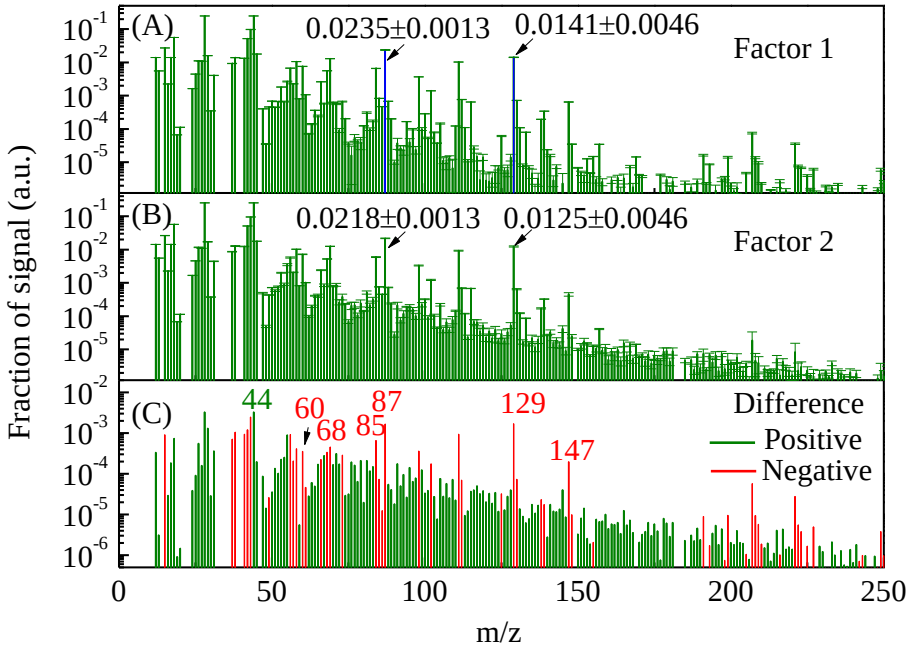


**Fig. 2.** Normalized mass spectra of **(A)** citric acid (PMF factor 1), **(B)** citric acid oxidation products (PMF factor 2), and **(C)** the difference mass spectrum (factor 2 – factor 1). The numbers in the upper two rows are the intensities of $m/z$ 87 and 129, while negative values are shown in the bottom row. The red and green lines indicate a negative and positive value, respectively.





ACPD
14, 8695–8722, 2014



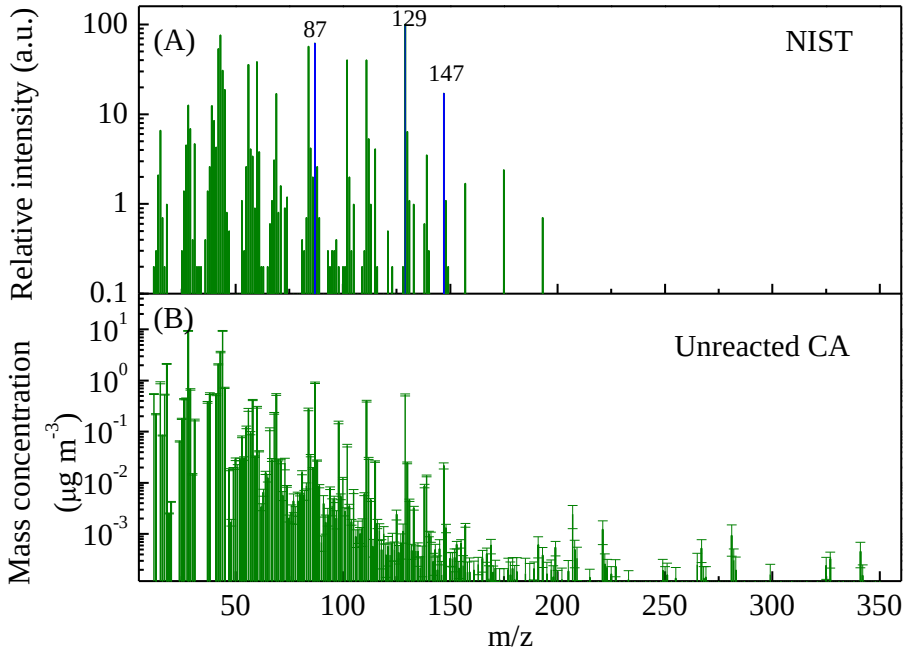


**Fig. 3.** Mass spectra **(A)** of CA from NIST database, **(B)** of pure CA measured with the C-ToF-AMS.





ACPD
14, 8695–8722, 2014



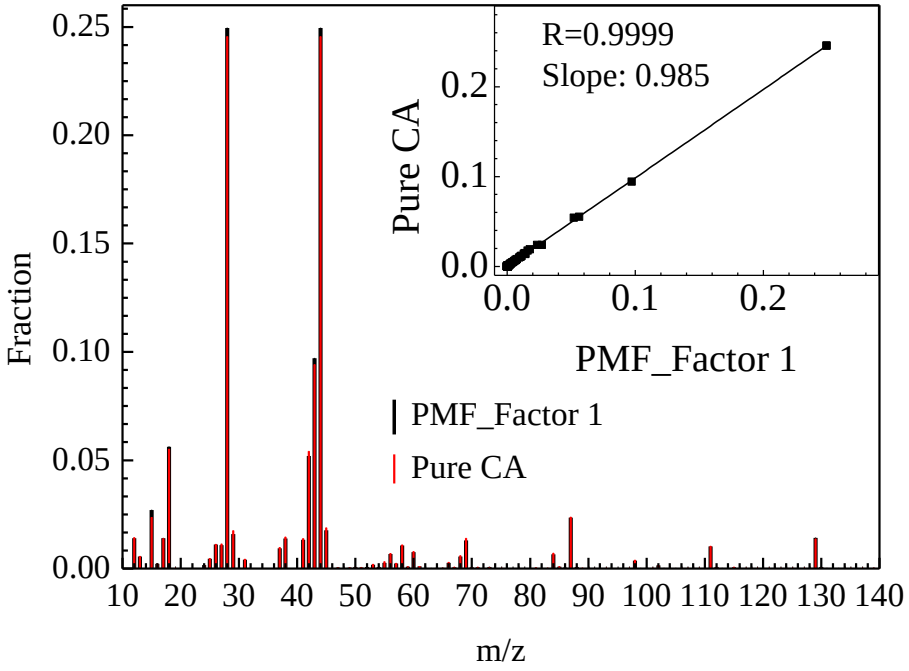


**Fig. 4.** Comparison between the mass spectra of factor 1 solved by PMF analysis and pure CA directly measured by C-ToF-AMS. The inset graph is the correlation of their corresponding signal intensity.





ACPD
14, 8695–8722, 2014



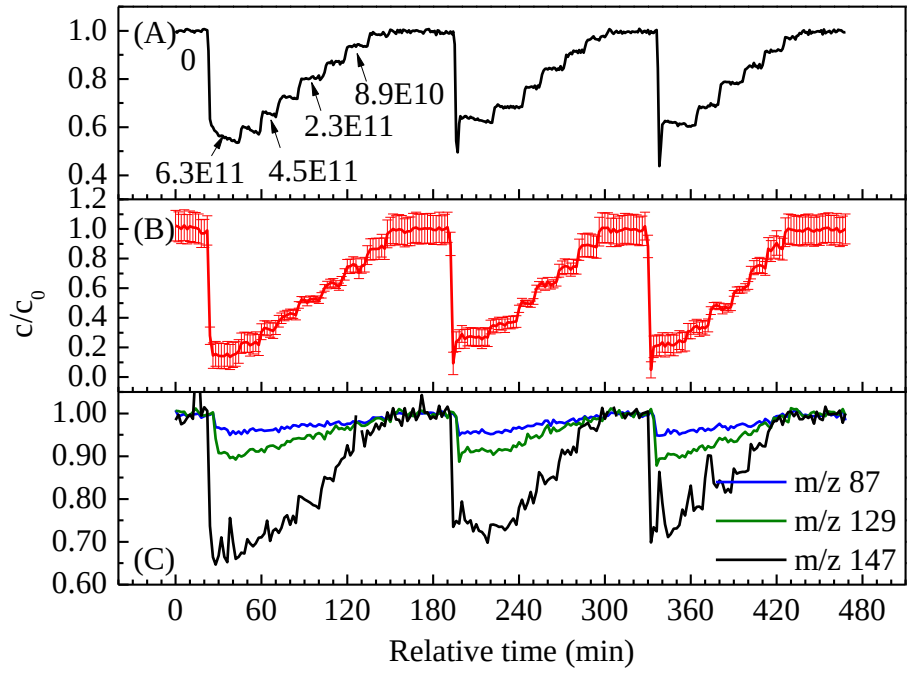


**Fig. 5.** Changes in the relative concentration of **(A)** methanol, **(B)** citric acid extracted with PMF analysis and **(C)** specific tracers measured with the AMS during the OH initiated oxidation of citric acid. Experimental conditions are $D_m$: 140 nm, RH: 30 ± 3 %, $T$: 298 K. The values in the top row represent the OH exposures.





ACPD
14, 8695–8722, 2014



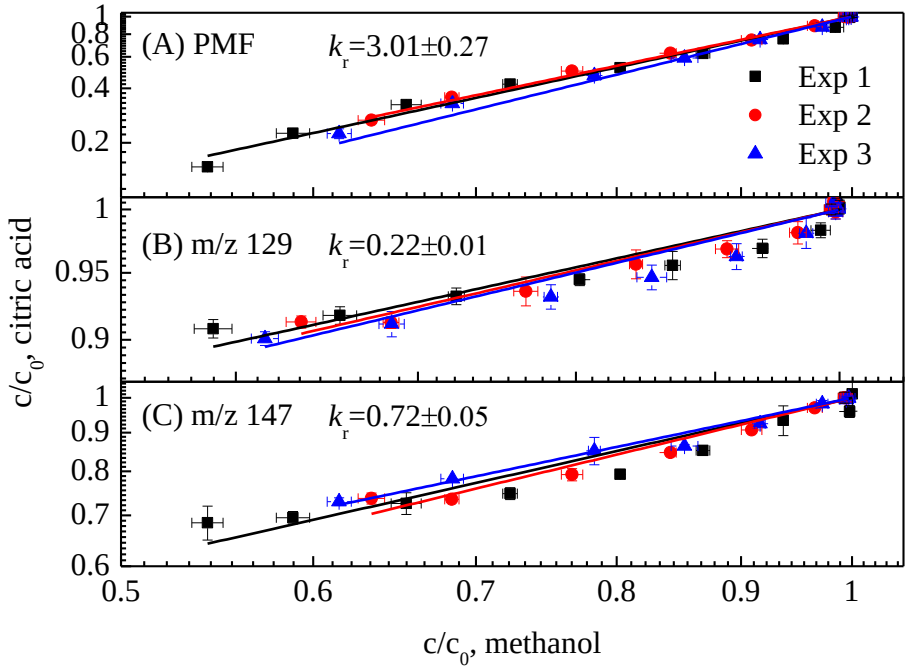


**Fig. 6.** Relative concentration of citric acid ($c/c_0$) as a function of the relative concentration of methanol based upon **(A)** PMF analysis, **(B)** $m/z$ 129 and **(C)** $m/z$ 147. Experimental conditions are $D_m$: 140 nm, RH: 30 ± 3 %, $T$: 298 K.





ACPD
14, 8695–8722, 2014



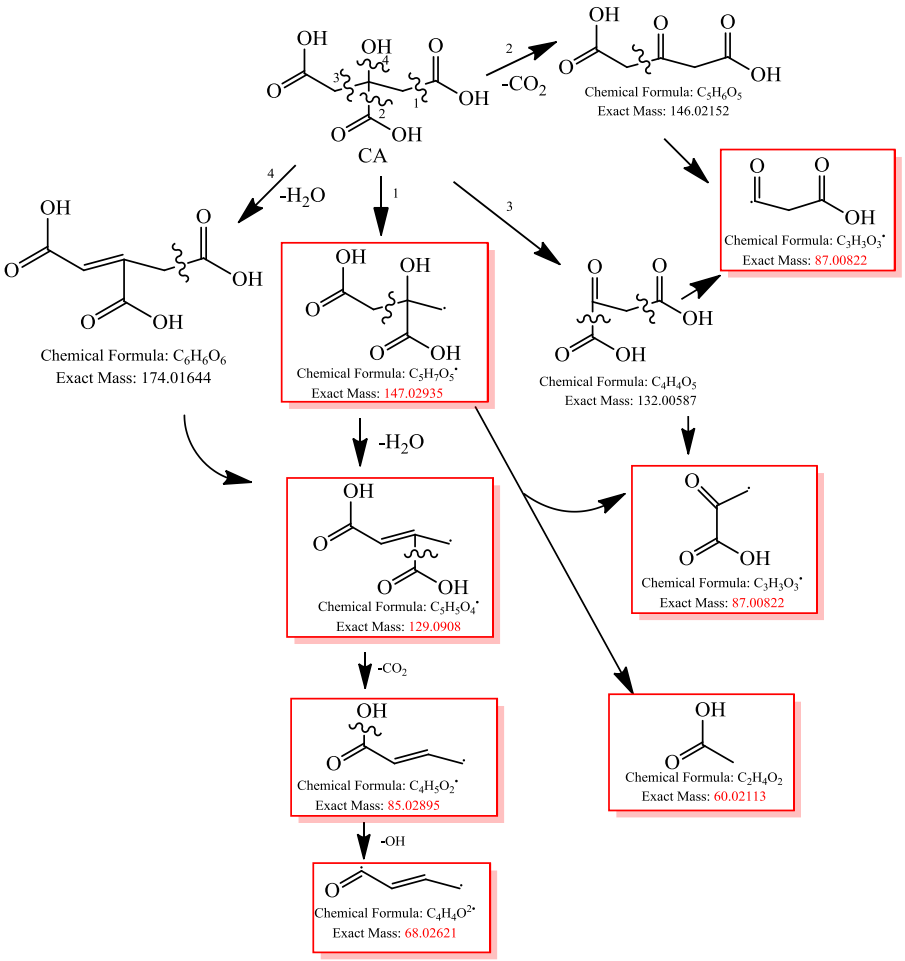


**Scheme 1.** Possible fragmentation pathways for citric acid.





ACPD
14, 8695–8722, 2014

Application of positive matrix factor analysis

Y. Liu et al.



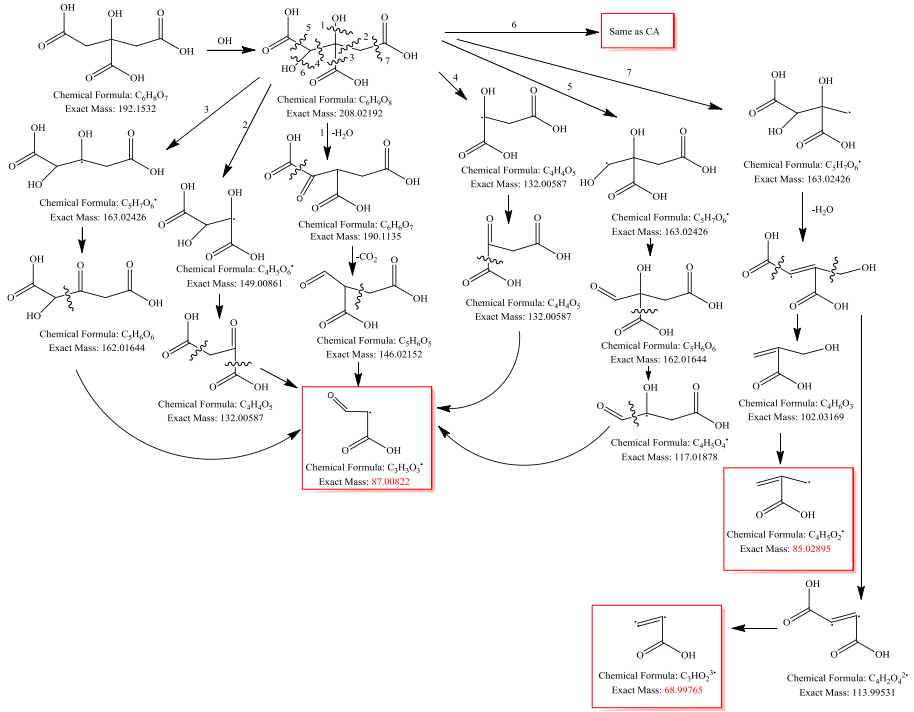


**Scheme 2.** Possible fragmentation pathways for an oxidation product of citric acid.





ACPD
14, 8695–8722, 2014